Optical Planet Discoverer: how to turn a 1.5-m telescope into a powerful exo-planetary systems imager

Bertrand P. Mennesson, Michael Shao, Bruce Martin Levine, J. Kent Wallace, Duncan Tsuen-Hsi Liu, et al.

Bertrand P. Mennesson, Michael Shao, Bruce Martin Levine, J. Kent Wallace, Duncan Tsuen-Hsi Liu, Eugene Serabyn, Stephen C. Unwin, Charles A. Beichman, "Optical Planet Discoverer: how to turn a 1.5-m telescope into a powerful exo-planetary systems imager," Proc. SPIE 4860, High-Contrast Imaging for Exo-Planet Detection, (3 March 2003); doi: 10.1117/12.457646

SPIE.

Event: Astronomical Telescopes and Instrumentation, 2002, Waikoloa, Hawai'i, United States

Optical Planet Discoverer: How to Turn a 1.5 m Telescope into a Powerful Exo-planetary Systems Imager

Bertrand Mennesson, Mike Shao, Bruce M. Levine, James K. Wallace, Duncan T. Liu, Eugene Serabyn, Stephen C. Unwin and Charles A. Beichman

Jet Propulsion Laboratory, California Institute of Technology, 4800 Oak Grove Drive, Pasadena CA 91109

ABSTRACT

Optical Planet Discoverer (OPD) is a 1.5 m class space telescope concept working as a visible nulling-interferometer imager. It is designed to detect Jupiter-like planets orbiting main sequence stars 10 pc away in a few minutes of integration and carry out a low resolution ($\simeq 20$) spectroscopy of their atmosphere. OPD would fit in the budget envelope of a discovery class mission. It would serve as an efficient precursor to a Visible Terrestrial Planet Finder (VTPF), a scaled-up 4 m class version based on the same optical scheme and allowing direct detection of 10 pc Earthlike planets in a few hours. We detail here OPD's optical principle layout, which is primarily driven by an *integrated* stellar light attenuation of 1e-6 in the final focal plane. The optical concept is based on a double-shearing nulling interferometer followed by an array of single-mode waveguides. The waveguides array ensures high residual starlight suppression - as already demonstrated at the 1e-6 level by preliminary JPL visible LASER nulling experiments - together with diffraction limited imaging of the circumstellar environment over a $\simeq 2$ arcsec field. During the observations, the telescope is spun around the line of sight to allow for proper detection of fixed planetary signatures against residual off-axis speckle patterns at the 1e-9 level. Use of the single-mode waveguide array to filter out scattered starlight eliminates the requirements for pristine $\lambda/4000$ rms wavefronts anywhere in the optical train. With OPD, stringent phase requirements apply only to scales larger than 5 cm - the equivalent size of the pupil regions to be recombined and nulled in a given fiber -, so that phase specifications can be met using low order active optics.

Keywords: extrasolar planets, interferometry, nulling, high dynamic range imaging, single-mode fibers, adaptive optics

1. INTRODUCTION

First concepts[1,2] suggested for the DARWIN and Terrestrial Planet Finder (TPF) space mission[3,4] relied on nulling interferometry in the thermal infrared. Alternative approaches using a single aperture coronagraph have also been suggested more recently[5,6] in the visible, with a slightly different expected scientific return.[7] The technical challenges are great in both cases. In the first case, one faces a huge background -of thermal and zodiacal origin- that needs to be monitored and subtracted with extreme accuracy during the observations. In the second case, the main difficulty consists in reaching the higher contrast -typically 10^{10}- expected in the visible between a solar type star and its potential Earth-like companion.

OPD is a shearing nulling visible interferometer: it lies somewhere in between the two approaches cited above. It operates in the [500 nm, 1000 nm] spectral region with broad-band imaging and low resolution ($\simeq 20$) spectroscopy capabilities. It uses nulling interferometry and spatial filtering through single-mode guided optics in order to reach the required very high rejection ratios on stars of finite angular size. Keeping the integrated leak over the whole focal plane to a value lower than $\simeq$ 1e-6, the fraction of stellar photons leaking at the planet's image location drops down to $\simeq$ 1e-9. At the same time, OPD takes advantage of the visible approach:

Further author information: (Send correspondence to B.M.)
B.M.: E-mail: bmenness@huey.jpl.nasa.gov, Telephone: 1 818 393 5466

High-Contrast Imaging for Exo-Planet Detection, Alfred B. Schultz, Richard G. Lyon, Editors, Proceedings of SPIE Vol. 4860 (2003) © 2003 SPIE · 0277-786X/03/$15.00

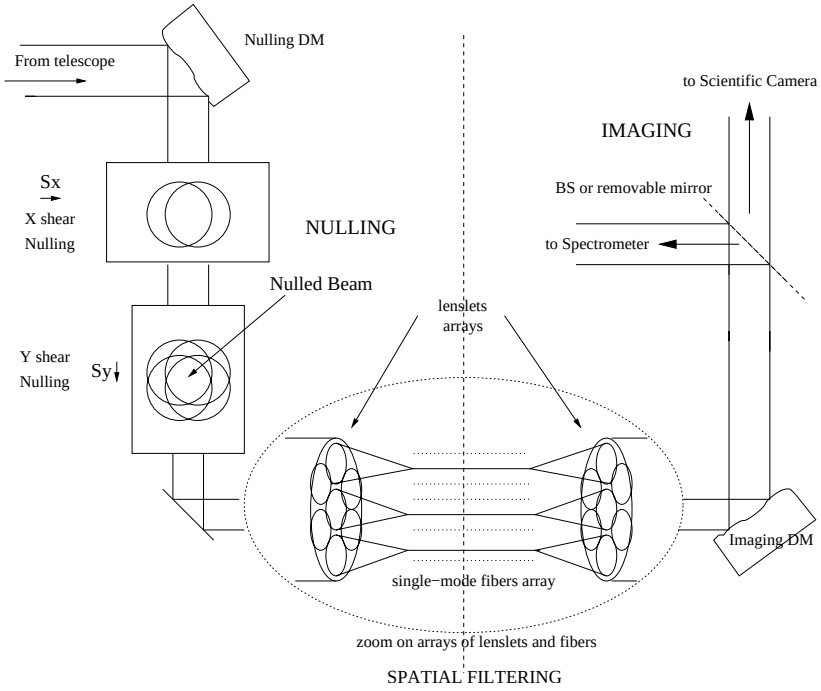

Figure 1. OPD schematic optical layout. The incoming light goes through three consecutive stages: nulling, spatial filtering and imaging (see text for details).

low background, direct imaging capability, higher spatial resolution for a given aperture and very low noise detectors.

In the next section we give a principle description of OPD's optical concept and derive some of the basic requirements for its proper operation. In sections 3 and 4 we present preliminary laboratory and simulation results in relation to some of OPD's subsystems. Finally we present in section 5 the expected scientific return of OPD. This discovery class mission would be mainly dedicated to the detection and spectroscopy of exo-Jupiters located in the region extending from about 2 to 10 A.U. away from their parent star. OPD is also directly scalable to a more sensitive 4 m version, meeting the requirements of the TPF mission (see Shao et al. in these proceedings).

2. OPD: A SHEARING NULLING IMAGER

2.1. Optical concept: principle design

OPD uses a 1.5 m class telescope, preferably with an off-axis primary - better suited to a shearing scheme -, which delivers an afocal beam, as represented in figure 1. The image formation process in the visible nuller follows three consecutive steps: the nulling-shearing part, mixing 4 sub-aperture beams with relative phases properly adjusted to create on-axis light cancellation, the spatial filtering stage using an array of single-mode waveguides to further suppress the stellar residual light, and the imaging system per se, detecting the resulting intensity distribution in the final focal plane and/or conducting low resolution spectroscopy.

2.1.1. Nulling

The collimated beam coming from the telescope hits a first beam splitter (figure 2). The 2 subsequent wavefronts are then phase shifted and laterally sheared with respect to each other. A quasi achromatic state of destructive interference - for an on-axis source- is obtained in the overlap region of the 2 beams by using a set of dielectric plates with properly adjusted thickness and refraction indices.[8] The amount of shear is controlled by the

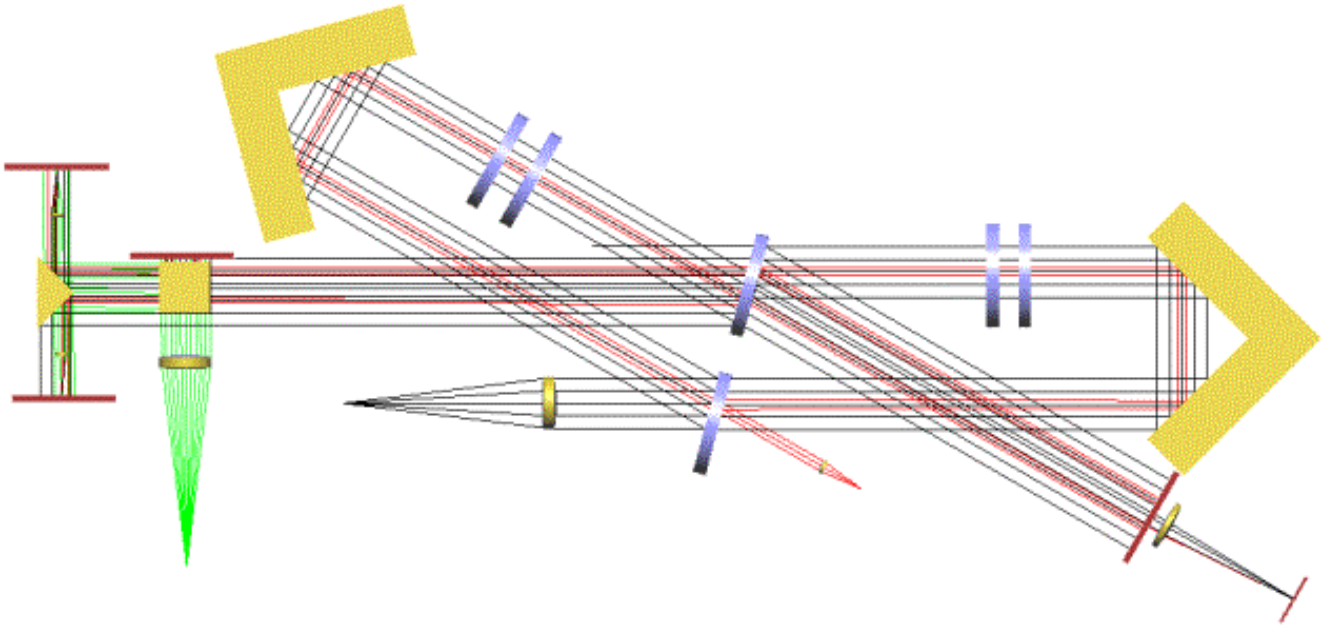

Figure 2. Principle of the shearing nulling interferometer. A quasi achromatic null is produced using a set of two dielectric plates in each arm. In this simplified version, which is the basis of a just starting new lab experiment at JPL, the optical path difference is controlled by translating one of the rooftops along the beam, whereas the other one fixes the shear. Note the metrology signal (lambda = 1319 nm) which is injected into the backside of the main beamsplitter (on the side opposite the white-light entrance into the nuller).

position of a rooftop located in one of the beams. The 2 beams are mixed through a beam combiner strictly identical to the first beam splitter, but oriented up-side down to preserve symmetry betweeen the beams. The resulting beam goes through a second analogous "shearing and nulling module", but with the shear occuring along the orthogonal transverse direction (figure 1). A mask is used to only retain the overlap region that is obtained after these two shears, defining the nulled beam. In the simplest case the amounts of shear are equal in both transverse directions, so that the final nulled beam traces back to 4 subapertures on the primary, equally spaced and nulled according to an "Angel cross".[9] A deformable mirror -nulling DM in figure 1- allows to match the optical path differences between the 4 beams to be destructively recombined.

2.1.2. Spatial filtering

Once the 4 beams are mixed and nulled, one could directly form an image of the astronomical source at this point, but the integrated starlight leak would be prohibitive (typically 1e-2) due to wavefront mismatches between the 4 beams. To be more specific, in order to get the desired integrated null of $\simeq$ 1e-6, one would need to recombine beams with a typical Strehl ratio of 0.999998 in the visible. In fact, in order to eliminate the amount of starlight scattered in the final image by the various optical surfaces, one first needs to inject the stellar beam into single mode waveguides. In that case wavefront mismatches between the beams are traded against amplitude mismatches inside each waveguide. These are of secondary effect on the achievable null depth. More precisely, one can show[11] that for small residual phase defects, the achievable null depth goes as σ_ϕ^4, the square of the wavefront variance when using single-mode waveguides -, instead of the conventional σ_ϕ^2. For a given wavefront amplitude and phase profile, much deeper stellar light cancellation is then achievable when single-mode waveguides are used. This represents a huge advantage, in fact already identified a long time ago.[10] Single-mode waveguides also have the advantages of broad-band utilization -the injection efficiency is roughly

achromatic over an octave- and perfect amplitude profile matching of the wavefronts to be nulled out. These single-mode waveguides can be either single-mode fibers, as already used for ground based interferometry,[12] or integrated guided optics - such as those obtained through ion exchange methods and also recently tested on astronomical telescopes.[13] Although the latter may ultimately be preferred -for its potentially greater stability and compactness- we only discuss hereafter a solution based on single-mode fibers, which are more readily available.

Now if one were to inject the nulled beam into one single-mode fiber only, any spatial information on the incoming field would be lost and no image could be recovered. The solution consists in using an array of single-mode fibers to preserve a moderate field of view and some spatial information. One can use an array of lenslets to subdivide the nulled beam (figure 1) into many contiguous "sub-pupils" of equivalent size d on the primary. For optimum results, this lenslets array has to be located in a pupil image plane. Each lenslet focuses a sub-pupil beam onto the head of a single-mode fiber. The optimal injection efficiency into a single-mode fiber is obtained for an f-ratio that matches the Airy spot and fiber core sizes, and this condition obviously has to be met for sensitivity reasons. In that case, it can be shown that the field of view FWHM seen by each fiber is essentially λ/d, where λ is the wavelength of observation. For instance, ensuring a 2 arscec FWHM field of view requires a sub-pupil equivalent size (assuming a magnification of 1) of 5 cm. After propagation and spatial filtering through the guides, the beams are re-expanded and collimated using a second matching lenslets array.

2.1.3. Imaging and spectroscopy

Once the stellar light has been cancelled at the 1e-6 level in each fiber, requirements for downstream imaging optics are considerably relaxed. Yet, the whole assembly of lenslets and fibers arrays needs to be adequately cophased (within $\lambda/20$ rms but with higher stability) to ensure sufficient image quality and stability in the final focal plane. This can be obtained through a second slowly deformable mirror dedicated to imaging (figure 1). Using a few hundred lenslets (hexagonally packed) and fibers, the final image PSF basically corresponds to an Airy pattern with a FWHM of $\lambda/(D-S)$ where D is the telescope diameter and S the amount of lateral shear (see section 4.2) .

Observations with the visible nuller are expected to be carried out in two phases. The broad-band detection phase using a small CCD matrix, and the spectroscopic phase, with a movable mirror allowing selection between the 2 instruments.

- Direct imaging. For maximum sensitivity a simple CCD matrix is used at the final focal plane conjugated to the second lenslet array. Nominal wavelength range is 500 to 1000 nm. Narrower filters may be implemented for specific observations. The field of view is λ/d ($\simeq$2") while the Airy pattern size is given by $\lambda/(D-S)$ ($\simeq$0.15" at 0.7 micron). Assuming 40 mas pixels, d=5 cm and D-S=1 m, 2500 pixels or e.g. a 64x64 CCD is enough. When working at -80 C, best CCDs have dark current as low as 1e-4 electron/s per pixel, and read-out noise of 2-3 electron rms per pixel. For each stellar type minimum individual integration times can then be chosen so that stellar residual shot noise dominates everywhere in the field. During the imaging phase, the telescope is rotated to allow proper distinction of planets versus optical defects.

- Low resolution spectrometer. Once planets have been detected and located with maximum sensitivity, a movable mirror sends the scientific beam towards a spectrometer. Two types of spectrometers are possible, one is a "long" slit spectrometer, where the slit direction is aligned in the direction of maximum planet throughput. The second is an integral field spectrometer that would measure the spectra of every object in the field.

  In the latter case, an image is formed on a 2-dimensional bundle array of $\simeq ((D-S)/d)^2$ i.e 400 multi-mode fibers. These are rearranged along one direction to allow spectral dispersion in the perpendicular one. A final CCD matrix using 800 pixels in the spatial dimension and 15 in the spectral one is enough to carry-out integral field low resolution (20) spectroscopy in the 500-1000 nm range. Note that depending on the source location, the input spectrum is modified by the nuller chromatic fringe pattern, an effect that can be easily calibrated.

2.1.4. Specific advantages

There are several advantages linked to the approach schematically depicted above. Some are given here, but a more detailed comparison can be found in Shao et al. in these proceedings.

- Easier wavefront correction.
  Any very high dynamic instrument working in the visible will face stringent wavefront requirements. The single-mode waveguide approach only places a strong requirement on equivalent scales larger than $\simeq 5$ cm, i.e. only on small spatial frequencies, for which an AO system with a limited number of actuators (a few 100) is sufficient. Such a single-mode filtering scheme looks very difficult to implement with a coronagraph.

- Smaller aperture.
  In a conventional coronagraph, a Lyot mask or apodized Lyot mask is used to block out the central part of the field. As the mask size decreases, its diffractive effects increase, and a larger Lyot stop is needed, so that the optimum mask size is of the order of 4-5 λ/D, where D is the diameter of the telescope aperture. For OPD the shear S is a fraction of the telescope diameter, typically one third, and any source lying outside of the deep nulled central region of the field can be imaged. This includes sources as close to the optical axis as $\lambda/2S \simeq 1.5\ \lambda/D$, which corresponds to 150 mas at 500 nm. With OPD, a smaller aperture size is then needed to provide a given angular resolution.

- Less sensitive to source angular size.
  All coronagraphic schemes suggested so far have a theoretical null depth proportional to $(D.\theta)^2$ where θ is the source angular size, leading to prohibitive stellar leakage for nearby stars with a 2 m or plus aperture. OPS's null depth varies as $(S.\theta)^4$ providing very deep theoretical nulls on the nearest stars as well. In addition, in a shearing nulling interferometer, the resolving baseline B=S.$\sqrt{2}$ (fixed by the amount of shear S) and the size of the effective aperture (D-S) are different. They can be easily adjusted from one star to another.

2.1.5. Key requirements

The fraction of stellar photons leaking through the final focal plane at the planet's image location needs to be kept below 1e-8 for sensitivity reasons. As we will see in section 4.2, we expect the stellar residual light to be scattered over the whole field (of size $\simeq \lambda/d$), whereas the planet's flux will concentrate in an Airy spot of FWHM given by $\lambda/(D-S)$. Owing to this spatial dilution effect, and using for instance 100 waveguides to pave the output pupil, a null depth of 1e-6 (integrated over the whole focal plane) is enough: it translates into a mean residual level of 1e-8 at the planetary location. OPD will use a few hundred fibers, so we will assume in the following that an integrated null depth of 1e-6 is appropriate.

Due to the use of single-mode fibers, the only limitations to the achievable null depth are: non zero relative optical path difference (opd), intensities and polarization mismatches between the 4 beams to be nulled out in a particular pupil lenslet or fiber. Table 1 presents the error budget and corresponding requirements to reach a 1e-6 null level. These specifications must hold for any particular 5 cm lenslet pupil.

The primary effect of a global pointing error α of the telescope is to offset the star by α from the perfectly nulled direction (it does not create any differential tilt between the subapertures wavefronts). It then can be regarded as an opd issue, and corrected as such by the fringe tracker. It may alternatively be taken care of at the telescope level by accurate pointing. Close to the optical axis the stellar leaks limit the null depth to an upper value[9]:

$$N = \frac{(\pi.B.\alpha/\lambda)^4}{16} \tag{1}$$

At a wavelength λ=500 nm, using a 70 cm baseline, one must keep the pointing jitter smaller than 3 mas to keep $N < 1e-6$. The specification on the pointing is then about 1mas rms. This should be accessible thanks to a small tip/tilt mirror located before the nulling assembly and using bright (e.g near infrared) stellar light for fast ($\simeq 100$ Hz) closed loop correction.

Table 1. Optical constraints on the relative phases, amplitudes, and polarizations of the 4 beams to be nulled out, assuming an integrated null depth of 1e-6 in the final focal plane.

Type of defect	Max. contribution to null depth	Corresponding requirement
Piston (non zero residual OPD)	4e-7	140 pm rms @ 700 nm
Overall intensity relative mismatch	3e-7	2.2e-3
Differential phase shift between polarizations	1.5e-7	1.1e-3 rad
Differential rotation of polarization planes	1.5e-7	7.6e-4 rad

2.2. Practical issues

- Polarization

  Best results obtained so far with a visible nuller[14] used one polarization only. OPD uses a different and very symmetric beam combination design (based on two identical up side down beam-splitters), which is expected to provide full dual polarization nulling capabilities.[15] This was already verified in the laboratory at the 1e-3 null level with a mid-infrared white light source: no influence of polarization was detected at this level with the Modified Mach Zender concept.

- Differential opd

  Residual piston (non zero opd) between the electric fields to be mixed in a common lenslet pupil will have to be actively corrected by a deformable mirror formed of 4 zones, each of them associated with one sub-aperture and using one actuator per lenslet pupil, i.e. roughly 500 to 1000 actuators. This zero-th order wavefront correction at the lenslet pupil level corresponds to a low spatial frequency (at the 5 cm scale) correction on the primary. Sensing could be carried out on each of the fiber signals, dithering around the visible nulls or at an other wavelength where stellar leaks are much higher. Additional LASER metrology may also be required. Getting down to the $\simeq$ 100 pm rms requirement -for these spatial scales only- is clearly the hard part of OPD. Note however that if no single-mode fiber were used to further clean the wavefronts, a Strehl ratio of 0.999998 and tens of thousands of actuators would be required to achieve the same required null depth of 1e-6.

- Intensity matching.

  Intensities from the various beams are not expected to vary rapidly with large amplitude. The largest effect expected -due to residual internal vibrations- comes from tip-tilt error fluctuations at the lenslet pupil level. Wavefronts arriving on a particular lenslet pupil with differents slopes are injected into the single-mode fiber with different efficiencies, which causes intensity mismatches and stellar leakage. In order to limit this effect at the required level (2.2e-3, from table above), and assuming no active intensity matching control device, individual beam directions must be kept within $0.014\lambda/d$ or 40 mas rms at λ=700 nm with 5 cm cells. This is actually much larger than the pointing requirement for the whole telescope. It may then not be necessary to implement any active intensity matching device.

3. RELEVANT LABORATORY RESULTS AND ON-GOING EFFORTS

3.1. Nulling

Several optical concepts have already been suggested and tested in order to produce deep achromatic or quasi-achromatic nulls.

3.1.1. The field flip approach

Deep nulls in the visible have been previously demonstrated at JPL using a rotational shearing interferometer. An achromatic field-flip between the interfering beams is obtained by using two orthogonal rooftops[14] or a pair of periscopes.[15] Stabilized nulls have been obtained with white light at the 1e-4 level with a 18% bandwidth using this technique. Transient nulls at the 1e-6 level and stabilized nulls at the 1e-5 level have also been obtained more recently on a LASER source (Martin et al. in these proceedings) using a single-mode fiber for spatial filtering. This was obtained for one polarization and without active control of the beams relative intensities. These results are very encouraging for OPD. They show that in the simple case of LASER light, we are already just one order of magnitude away from the requirements. They also clearly validate the single-mode waveguide approach: LASER nulls measured under the same conditions but without visible single-mode waveguides did not exceed 100!

3.1.2. The dielectric plates approach

In the case of 4 beam combination, the aperture flip technique has the deleterious effect of interfering portions of the entrance pupil that are in general not located on a regular cross - i.e. with orthogonal arms crossing at their centers. This results in slightly increased leaks for a source of finite diameter (Mennesson in preparation) as compared to the perfect Angel cross. This subtle effect can be neglected as long as the apertures to be recombined are small compared to the interferometric baseline. This would be the case for a large space infrared nulling interferometer, but clearly not for OPD. Consequently, we decided to use a nulling scheme based on dielectric plates rather than a geometrical field and aperture flip. In that case a quasi-achromatic π phase shift is obtained locally in a given wavelength range by using a proper set of glasses, with carefully matched refraction indices and thicknesses. The same design has been chosen for the Keck nuller mid-infrared atmospheric dispersion corrector (Koresko et al. these proceedings). It already produced encouraging preliminary results in the lab with transient broad-band (18% bandwidth) nulls at the 1e-3 level (Serabyn et al. in these proceedings, Mennesson et al. in preparation). Figure 3 gives as an example the theoretical phase shift and corresponding null depth accessible using a set of BK7 and fused silica glass plates of appropriate thicknesses.[8] This shows that nulls constantly better than 1e-6 can already be obtained on the 500 nm to 800 nm region with conventional glasses. This also suggests that a visible / near IR dichroic and two dedicated nulling channels may be necessary for proper operation of OPD over the whole 500 to 1000 nm range.

3.1.3. Lenlets and single-mode fiber arrays

Two laboratory experiments have just been engaged at JPL to demonstrate OPD key technologies. The first one concentrates on the high rejection requirement. It aims at testing the shearing nulling concept based on dielectric plates, as described above and schematically presented on figure 2. It uses only one single-mode fiber for spatial filtering and its goal is to achieve 3e-7 stabilized nulls on a thermal source with 300 nm bandwidth. The second aims at proving the imaging concept. It uses two arrays of lenslets - hexagonally packed with a 125 micron pitch, and a fibers bundle. For alignment purposes, fibers with a large core size (typically 30 microns) and a small numerical aperture are preferred. A small $\simeq$ 5x5 array of photonic cristal single-mode fibers (core radius of $\simeq$ 30 μm) will first be tested for imaging purposes.

4. SIMULATIONS

OPD can be considered as a regular imaging system but seeing the sky through a transmission grid set by the nulling stage.

4.1. Nulling

Figure 4 gives the monochromatic (λ=500 nm) sky transmission pattern for OPD, assuming a 50 cm shear S, i.e. a 70 cm baseline B. Note that this instrument becomes reasonably sensitive for sources as close as 70 mas to the optical axis. The transmission grid Tr over the sky is the product of the Angel's cross fringe pattern,[9] apodized by a function ρ describing the "lobe antenna" of a single-mode fiber. ρ corresponds to the coupling efficiency into the fiber, which is a function of the source coordinate on the sky and the f-ratio. The f-ratio is set to the value optimizing the coupling efficiency of the light from an on-axis point source into a single-mode

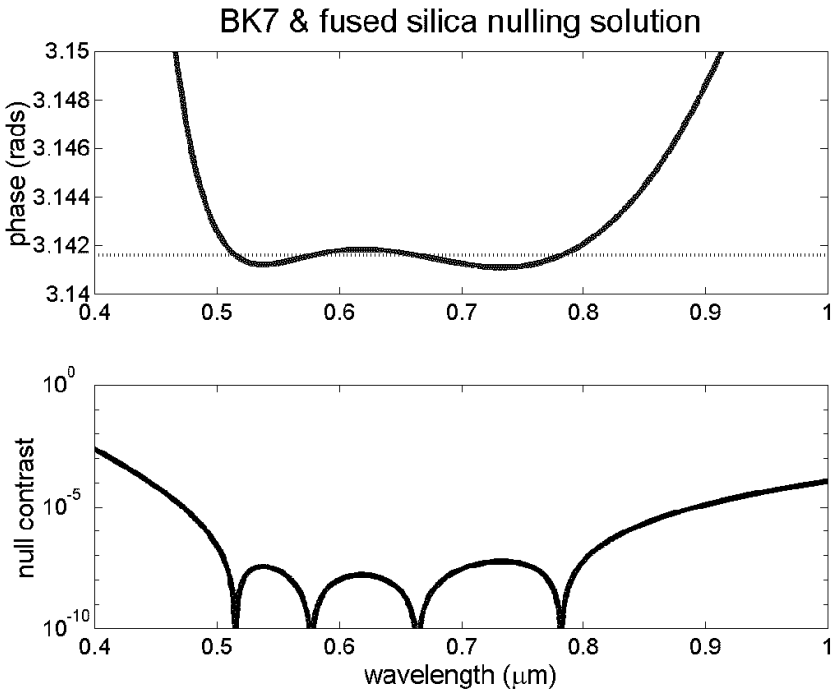

Figure 3. Top: Phase shift obtained in the [500, 1000 nm] range with an optimized combination of two glasses: BK7 and fused silica. Bottom: Resulting null level.

fiber. In that case the field of view common to all fibers is essentially limited to one Airy pattern set by the sub-pupils diameter d, and ρ varies across the field according to the analytical expression derived by Guyon.[16]

$$Tr(\theta_x, \theta_y) = (1/4)[cos(\pi.B.\theta_x/\lambda) - cos(\pi.B.\theta_y/\lambda)]^2.\rho(\theta_x, \theta_y, d, \lambda) \quad (2)$$

where θ_x and θ_y refer to the sky angles along each of the shearing directions x and y. The average transmission over the sky is 25%. Note that there are some holes in the transmission pattern, so that one will need to rotate the array to be able to image planets at these locations. One could also have different shears along the 2 directions to get a more uniform sky coverage after rotation, as originally suggested by Angel.

Integrating equation (2) over a stellar disk of extent $\Delta\theta$, one can show that the relative stellar leakage, i.e. the null depth N amounts to:

$$N(\Delta\theta) = \frac{1}{1536}(\pi.B.\Delta\theta/\lambda)^4 \quad (3)$$

Normalizing to the case of OPD with a 1 mas diameter star (a Sun at 10 pc has an apparent diameter of 0.9 mas), seen at 500 nm, with a 0.7 m baseline (0.5 m shear S), we get:

$$N = 1.3\,10^{-10}.(\Delta\theta^*_{mas})^4.(\frac{0.5}{\lambda_{\mu m}})^4.(\frac{S_{in\,m}}{0.5})^4 \quad (4)$$

Ensuring theoretical stellar leaks smaller than 1e-8 at 500 nm on Procyon (closest F star) which is about 3 mas in angular diameter requires a shear S smaller than 0.5 m. Conversely, for a 0.5 m shear (0.7 m baseline), the first constructive peak is obtained at an off-axis angle $\lambda/B \simeq 150$ mas at 500 nm. The OPD value S=0.5 m provides a comfortable theoretical null even for the nearest main sequence stars. At the same time it ensures a good sensitivity over the whole [500 nm, 1000 nm] spectral range for any source located 150 mas away or more from its parent star.

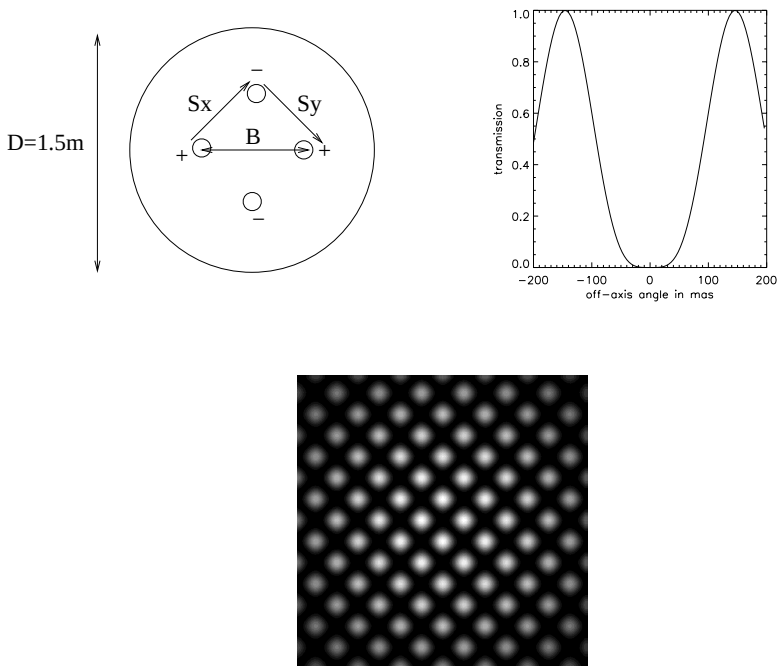

Figure 4. Top left: The 4 individual nulled beams which are seen by a given lenslet trace back to 4 spatially separated beams on the primary, forming an Angel cross with baseline B=S.$\sqrt{2}$. Top right: Monochromatic transmission pattern along the B direction for B=0.7;m, λ=500 nm . Note the flat central response. Bottom: 2-dimensional monochromatic transmission grid over the sky, same assumptions. Field of view is 2 arcsec in diameter.

4.2. Imaging

We carried out a few preliminary simulations to look at the expected PSF of the system in a particular case: D=1.5 m, S=0.5 m, d=5 cm, which yields to an array of 293 lenslets and fibers. Assuming that the array is cophased within $\lambda/10$ rms, and just modeling this piston effect, one gets a PSF that is very close to the diffraction pattern of the nulled beam aperture, i.e. a FWHM given by $\lambda/(D-S)$. Of course a realistic simulation should introduce higher order wavefront corrugations, but these will be mostly static and easy to distinguish from planetary signatures. Their effect is also very limited as long as the stellar light has been adequately nulled in each fiber.

More interestingly we simulated the residual stellar signal in the final focal plane. For this we assumed that each fiber's electric field amplitude was at a level 1e-3 relative to the constructive case, and affected by an rms 1e-3 - a negative amplitude being interpreted as a π additional phase. If the residual leaks are OPD related, one can indeed show that the leak average and rms levels are close to each other. Now comes the question of the relative phases of all these quasi-nulled stellar electric fields. The only way to get a centrally peaked residual stellar image in the focal plane is to have all these phases very close to each other, which is very unlikely. In fact these phases are ill-defined, and should be completely random in the general case, because there are the phases of quasi null electric fields. Looking more closely, the phase of the nulled stellar beams only relate to the incoming wavefront phase when either amplitude mismatch, or opd mismatch *systematically* dominate the residual nulls in *all* of the fibers. For instance, it would require that the amplitude coming from a given portion of the primary be always greater. This is very unlikely since most of the amplitude fluctuations should come from residual tip/tilt on the fiber's head. In any case the peak speckle levels are of the order of 1e-8 at the max. With the fair assumption that the stellar electric fields transmitted by each fiber have random relative phases, one gets an instantaneous image as presented in figure 5a, with the star residual light randomly distributed in the focal plane. The speckles are created by the intensity fluctuations from one fiber to an other,

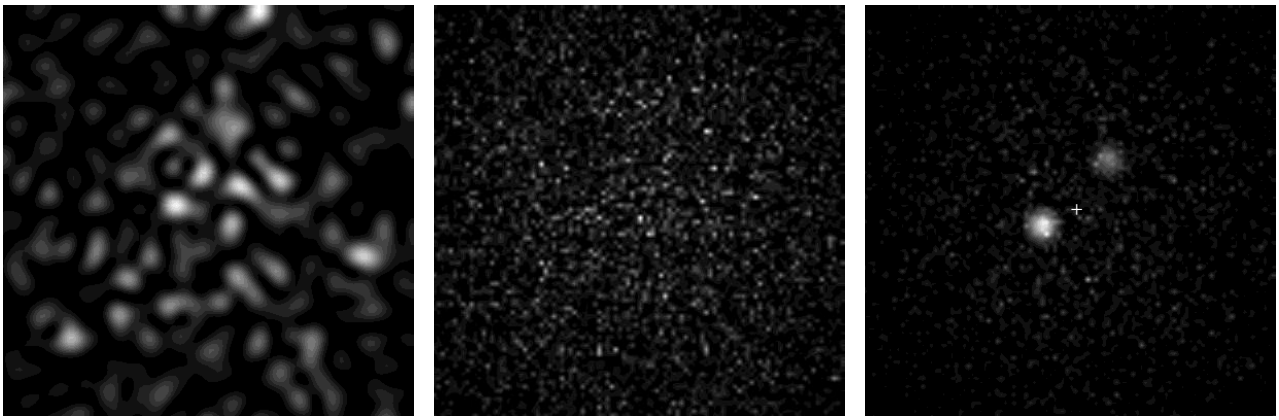

Figure 5. Simulations of focal plane images obtained with OPD. FOV is 2 arcsec in diameter, pixel size is 20 mas. (a): instantaneous speckle pattern (star only). (b): summation of 5 independent stellar snapshots. (c): simulation of the 47 Uma planetary system as seen over a 10 minute exposure. The central cross denotes the position of the star. See text for details.

evolving rapidly in time with vibrations and pointing jitters. The field of view is 2 arcsec in diameter, the pixel size is 20 mas. The distribution is still slightly centrally peaked because of the individual fibers gaussian beam profile. As expected the typical size of each speckle is about $\lambda/(D-S)$. For the detector read-out noise to remain negligible, individual integration times will in fact be much longer than the speckle boiling time. It will range from a few minutes to a few hours, depending on the stellar brightness. Each frame will then see many realizations of the speckle pattern. Figure 5b shows the summation of just 5 independent speckle patterns, where the small spatial frequency structure appears to be broken. The maximum speckle level is now 8.3 e-9, the average is 7.9e-10, and the rms amounts to 8.4e-10. Finally figure 5c represents a simulation of the image that would be obtained while observing the G0V star 47 Uma. From radial velocimetry measurements,[17] this star is known to host two giant planetary companions respectively 2.09 and 3.73 A.U. away. For this simulation, the system is assumed to be pole-on, so that the two planets appear 157 and 280 mas away from the optical axis. Each of the planet is assumed to have Jupiter radius and albedo. The simulated integration time is 10 minutes, the spectral range is 500 to 700 nm.

5. SCIENTIFIC OUTCOME

OPD is mainly dedicated to the low resolution spectroscopy ($\simeq 20$) of giant extrasolar planets. Even at this resolution one should be able to identify the absorption bands of methane, the most prominent of which is at 890 nm, evident in Jupiter and Neptune. Other specific spectral signatures may also be revealed as in the case of some hotter Jupiters, referred as "roasters"[19] where K or Na may be detectable in the 700 nm to 800 nm region.

5.1. Integration times for broad-band planetary detection

Broadband planetary detection would be carried out over the whole [500 nm, 1000 nm] spectral range. We derive in the following the integration times necessary to detect Jupiter "analogs" (with same planetary radius and albedo).

- Solar flux

  Sun absolute (i.e 10 pc) R magnitude is M_R=4.28, corresponding to a flux e(0.70μm)=3.42 $10^{-10} W.m^{-2}.\mu m^{-1}$. This translates into a photon flux received from 10 pc around 0.70 μm of:

$$(\lambda.N_\lambda)_{Sun} = 8.42\,10^8 photons.\ m^{-2}\,s^{-1} \tag{5}$$

- Jupiter flux and detection time

  A Jupiter analog, located 5.2 AU from a solar type star 10 pc away emits at 0.70 μm and full phase[18] a flux of 1.30 $10^{-18} W.m^{-2}.\mu m^{-1}$. When observed at quarter phase which is a more conservative assumption, the planetary reflected flux drops by a factor π to 4.14 $10^{-19} W.m^{-2}.\mu m^{-1}$ or:

$$(\lambda.N_\lambda)_{Jupiter} = 1.0\,photon.\ m^{-2}\,s^{-1} \tag{6}$$

Assuming that the 700 nm fluxes are representative of the whole [500,1000] nm range and that stellar photon noise dominates, a rough Signal to Noise Ratio (SNR) estimate is provided by the ratio of the detected planetary photons to the stellar photon count rms:

$$SNR = \frac{(\lambda.N_\lambda)_{Planet}.Reso^{-1}.A.T.Eff.Tr}{((\lambda.N_\lambda)_{Sun}.Reso^{-1}.A.T.Eff.sl)^{0.5}} \tag{7}$$

with Reso=$\frac{\lambda}{\Delta\lambda} = \frac{0.70\mu m}{0.5\mu m} = 1.4$ the spectral resolution, $A = \pi.D^2/4$ the collecting area for a telescope of diameter D, T the overall integration time, Eff the overall detection efficiency including partial use of the telescope surface area, optics transmissivity, injection efficiency into single-mode fibers and detector quantum efficiency, Tr the interferometric transmission at planetary location. The speckle level sl corresponds to the fraction of stellar photons leaking through the final focal plane at the planet's image location. Since the planetary position is a-priori unknown Tr should be taken equal to 0.25, the interferometric mean transmission over the sky. In fact, this is not correct. Each star is observed with 4 different rotation angles of the telescope, obtained by increments of 25 degrees. Post-processing of the data should allow to get rid of the exposures where the planet is blocked out by the nuller transmission grid. Optimum weighting of the four exposures results in an increased SNR with respect to the constant Tr=0.25 case - indeed the low Tr exposures only add noise. This effect was taken into account.

When normalizing to the nominal values for a discovery class mission: D=1.5 m, T=1 h, Eff=5% and sl=10^{-9} (assuming an integrated null depth of 1e-6), we get for a Jupiter analog orbiting a Sun-like star at a distance (Dist) of 10 pc:

$$SNR = 14.2(\frac{D_{in\,m}}{1.5}).(T_{in\,h})^{0.5}.(\frac{Eff}{0.15})^{0.5}.(\frac{10^{-9}}{sl})^{0.5}.(\frac{10}{Dist_{in\,pc}}).(\frac{1.4}{Reso})^{0.5} \tag{8}$$

Looking at the general case of an exo-Jupiter with a given separation Sep in A.U. from a central star with flux F^*, and assuming pure stellar reflection with Jupiter's albedo, we get:

$$SNR = 14.2(\frac{D_{in\,m}}{1.5}).(T_{in\,h})^{0.5}.(\frac{Eff}{0.15})^{0.5}.(\frac{10^{-9}}{sl})^{0.5}.(\frac{10}{Dist_{in\,pc}}).(\frac{1.4}{Reso})^{0.5}.(\frac{5.2}{Sep})^2.(\frac{F^*}{F_{Sun}})^{0.5} \tag{9}$$

and the integration time T_{int} for broadband detection of exo-Jupiters is:

$$T_{int} = 7\ mn\ .(\frac{SNR}{5})^2.(\frac{1.5}{D})^2.(\frac{0.15}{eff}).(\frac{sl}{10^{-9}}).(\frac{Dist_{in\,pc}}{10})^2.(\frac{Reso}{1.4}).(\frac{Sep}{5.2})^4.(\frac{F_{sun}}{F^*}) \tag{10}$$

One can note the strong dependency on the planetary separation. A Jupiter "analog" orbiting at 2 AU from a solar type star 10 pc away can be detected at 5σ in less than a minute.

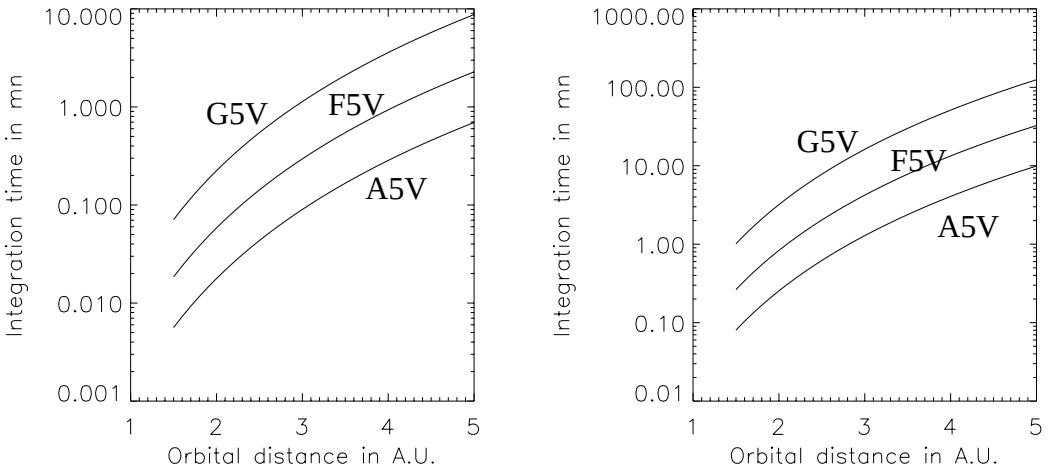

Figure 6. Theoretical integration times for 5σ broad-band detection (a) and low resolution (20) spectroscopy (b) of Jupiter like planets orbiting main sequence stars of various spectral types. See text for assumptions.

5.2. Integration times for low resolution spectroscopy

During the spectroscopic phase the planetary location has been determined, so that we use for Tr a value of 0.5. With a spectral resolution of 20 across the 500 to 1000 nm range we get the integration times for low resolution spectroscopy of Jupiter-like (same albedo and radius) planets.

$$T_{int} = 1.7\ hr\ .(\frac{SNR}{5})^2.(\frac{1.5}{D})^2.(\frac{0.15}{eff}).(\frac{sl}{10^{-9}}).(\frac{Dist_{in\,pc}}{10})^2.(\frac{Reso}{20}).(\frac{Sep}{5.2})^4.(\frac{F_{Sun}}{F^*}) \quad (11)$$

Note that significant atmospheric characterization can already occur at a spectral resolution as low as 5.

6. SUMMARY

We have presented a new concept for the direct detection and low resolution spectroscopy of giant extrasolar planets around the $\simeq 100$ nearest main sequence stars making use of a single 1.5 m telescope. OPD could be implemented as a Discovery class Mission, and serve as a potential technical and scientific precursor for a visible Terrestrial Planet Finder, based on the same design but extended to a larger$\simeq 4$ m aperture.

OPD builds up on previous (SIM visible nuller) and still on-going (Keck nuller) efforts conducted at JPL, that already validated to a large extent some of the key technologies suggested: spatial filtering through single-mode waveguides, opd control through dithering, deep achromatic nulling. In addition to the usual benefits of the visible approach (smaller aperture needed, low background, direct imaging capability, etc ..) OPD's nulling / spatial filtering scheme apparently brings specific and decisive advantages: no need for any active wavefront correction at spatial frequencies larger than $\simeq 20$ cycles/m, and high dynamic range imaging even around the nearest stars. These encouraging laboratory results and obvious advantages make us confident that OPD's technical requirements and ultimate scientific objectives are within reach of a dedicated effort. The apparent cost effectiveness of this approach also makes it very appealing for TPF, and at least worth investigating very seriously.

ACKNOWLEDGMENTS

The research described in this paper was carried out at the Jet Propulsion Laboratory, California Institute of Technology, under a contract with the National Aeronautics and Space Administration.

REFERENCES

1. Léger A., Mariotti J.M., Mennesson, B. et al. 1996, "Could we search for primitive life on extrasolar planets in the near future? The DARWIN project", Icarus **123**, 249-255
2. Mennesson B., and Mariotti M., 1997, Icarus, 128, 202
3. Angel J.R.P. and Woolf N.J., "An imaging nulling interferometer to study extrasolar planets", ApJ, **475**, 373-379 (1997)
4. Beichman C.A., Woolf N.J. and Lindensmith C.A., The Terrestrial Planet Finder (TPF): A NASA Origins Program to Search for Habitable Planets, JPL publication 99-3
5. Nisenson P. and Papaliolios C. 2001, ApJ 548, L201
6. Rouan D. et al., 2000, PASP, 112, 1479
7. DesMarais D.J. et al., Biosignatures and Planetary properties to be investigated by the TPF mission. JPL Publication 01-008, Rev. A, June 2002.
8. Morgan R., Burge J. and Woolf N. 2000, SPIE Conf. 4006, 340.
9. Angel, R. 1990, Proceedings of the Workshop on the NGST, P.Bely and C. Burrows Eds, STSCI, 81
10. Shao, M. 1991, SPIE Conf.Ser. 1494, Hubble Extra Solar Planet Interferometer
11. Mennesson B., Ollivier M. and Ruilier C., 2002, JOSA A, 19, 3, 596
12. Coudé du Foresto, V., Perrin, G., Ruilier, C., Mennesson B., Traub W. & Lacasse M., 1998, in SPIE Conf. Ser. 3350, Astronomical Interferometry, ed. R. Reasenberg (Bellingham: SPIE), 854
13. Berger J.P. et al. 1999, A&AS, **139**, 173
14. Wallace J.K., Hardy G., and Serabyn E., 2000, Nature, 406, 700.
15. Serabyn E. and Colavita M., 2001, Applied Optics, 40, 1668
16. Guyon O., 2002, A&A, 387, 366
17. Fischer D.A. et al., 2002, ApJ, 564, 1028
18. Karkoschka E. 1994, Icarus 111, 174
19. Sudarsky D., Burrows A. and Pinto P. 2000, AJ, 538, 885